

## Local structure of $\text{Co}^{2+}$ incorporated at the calcite surface: An x-ray standing wave and SEXAFS study

Likwan Cheng

*Department of Materials Science and Engineering, Northwestern University, Evanston, Illinois 60208  
and Environmental Research Division, Argonne National Laboratory, Argonne, Illinois 60439*

Neil C. Sturchio

*Environmental Research Division, Argonne National Laboratory, Argonne, Illinois 60439*

Michael J. Bedzyk

*Department of Materials Science and Engineering, and Institute of Environmental Catalysis,  
Northwestern University, Evanston, Illinois 60208  
and Materials Science Division, Argonne National Laboratory, Argonne, Illinois 60439*

(Received 15 October 1999)

Following adsorption from a dilute water solution, the lattice site and first-neighbor bonding distances of  $\text{Co}^{2+}$  ions incorporated at the calcite ( $10\bar{1}4$ ) surface were determined with atomic resolution by the combination of x-ray standing wave triangulation and polarization-dependent surface extended x-ray absorption fine-structure spectroscopy. The incorporated  $\text{Co}^{2+}$  ions selectively occupy the  $\text{Ca}^{2+}$  lattice sites with an inward relaxation of 0.34 Å. The  $\text{Co}^{2+}$  ions remain octahedrally coordinated, with a first-neighbor Co-O bonding distance of 2.11 Å. The octahedral coordination suggests that a coadsorbed species from the solution remains bonded to the  $\text{Co}^{2+}$  ion above the surface. The structure of  $\text{Co}^{2+}$  incorporated at the calcite surface is successfully described by a model in which the  $\text{Co}^{2+}$  sites are mainly determined by relaxation due to surface lattice asymmetry, and the first-neighbor Co-O relaxation by reconfiguration of the adjacent carbonate molecules.

### I. INTRODUCTION

Recent x-ray absorption fine-structure (XAFS) studies of several substitutional cation impurity structures in the calcite crystal ( $\text{CaCO}_3:M$ , where  $M = \text{Zn}^{2+}$ ,  $\text{Co}^{2+}$ ,  $\text{Ba}^{2+}$ ,  $\text{Pb}^{2+}$ ,  $\text{Mn}^{2+}$ , and  $\text{Sr}^{2+}$ ) revealed a characteristic, substantial local relaxation with preserved bonding coordination at the impurity sites.<sup>1-3</sup> The first-neighbor impurity-to-oxygen ( $M$ -O) distances approached those of the pure carbonate crystals of the respective impurity ions, i.e., the Pauling limit. This impurity structure observed in calcite, presumably also existing in similar molecular ionic crystals, is in sharp contrast to analogous impurity structures in monatomic crystals. For impurities in both ionic<sup>4-6</sup> and covalent<sup>7-9</sup> binary crystals, for example, the first-neighbor distances fall clearly between the Pauling and the virtual crystal approximation (VCA) limits. Similarly, for cation impurities in complex oxides that are stoichiometrically identical to  $\text{CaCO}_3$ , relaxation of neighboring anions is typically limited, and often accompanied by off-center shifts of the impurity ions.<sup>10</sup>

The remarkable degree of local relaxability without bonding disruption at the calcite impurity site is apparently the molecular-level basis of calcite's great capacity for isomorphic accommodation of foreign ions of various sizes. Since impurity ion incorporation in calcite occurs commonly by substitution at the liquid-calcite interface—an interfacial trace element transport process fundamental to many geochemical, environmental, and biomineralogical problems<sup>11</sup>—it is important to make direct observation of the

impurity structure at the calcite surface.

Combining the x-ray standing wave (XSW) and the in-plane surface extended x-ray absorption fine-structure (SEXAFS) techniques, we recently measured the atomic-scale structures of  $\text{Zn}^{2+}$  and  $\text{Pb}^{2+}$  impurities incorporated at the calcite ( $10\bar{1}4$ ) cleavage surface.<sup>2,12-14</sup> These studies demonstrated certain key similarities between a surface and a bulk impurity structure, i.e., the surface impurity is substitutional and observes in-plane conservation of the first-neighbor distances. However, further information is needed in order to construct a complete structural model. One question to be resolved is how the divalent impurity cation maintains its preferred octahedral coordination at a surface site. Another question is the transferability of the impurity structure, i.e., do all isomorphically incorporated divalent cations at the calcite surface have similar structures, as is the case for bulk impurities? This latter question requires a direct proof, since one experiment indicated that  $\text{Zn}^{2+}$  and  $\text{Co}^{2+}$  showed different incorporation mechanisms on the calcite ( $10\bar{1}4$ ) surface.<sup>15</sup>

To help answer these questions we carried out XSW triangulation and polarization-dependent SEXAFS measurements on isolated  $\text{Co}^{2+}$  ions incorporated at the calcite ( $10\bar{1}4$ ) surface. This combination of atomic-scale techniques permits measurements on both the position of the impurity ion relative to the substrate crystal lattice and the local bonding structure of the surface lattice relative to the impurity. Results obtained from this study are used to construct a clear atomic-scale structural model of an isomorphic substitution

at the calcite surface. This model indicates that a coadsorbate molecule is attached to the incorporated surface  $\text{Co}^{2+}$ . Furthermore, this  $\text{Co}^{2+}$  surface impurity structure is similar to that of  $\text{Zn}^{2+}$ .

## II. EXPERIMENTAL PROCEDURE

Calcite samples were prepared by cleaving optical-quality single crystals. A freshly cleaved (10 $\bar{1}$ 4) face was reacted with a dilute aqueous Co solution prepared from a 0.5 mM cobalt nitrate solution, pH 6.8, for approximately 5 min at room temperature. An amount of 0.55 mM ethylenediamine-tetraacetic acid was added to the solution to ensure that all solid Co phases were extremely undersaturated. Based on previous work on heteroepitaxial otavite-calcite solid solution formation on calcite,<sup>16</sup> it is believed that Co is incorporated at the calcite surface by a dissolution-precipitation mechanism occurring at step edges. After the adsorption reaction the solution was rapidly removed from the calcite surface using a jet of dry nitrogen gas. X-ray measurements were done in a helium atmosphere at room temperature.

The x-ray measurements were carried out at beamline X15A of the National Synchrotron Light Source. The procedures of these measurements were similar to those used previously for  $\text{Zn}^{2+}$  adsorption on calcite.<sup>14</sup> Certain instrumental settings and choices of data acquisition specific to the current measurements are given below.

The XSW measurements for calcite lattice site triangulation of the  $\text{Co}^{2+}$  ion were made with the [10 $\bar{1}$ 4] surface normal diffraction vector and the [01 $\bar{1}$ 8] and [2 $\bar{2}$ 04] off-normal diffraction vectors. The incident x-ray beam was tuned to 9.00 keV by a double-crystal Si(111) monochromator for the (10 $\bar{1}$ 4) measurement, and to 9.80 keV by a Si(220) monochromator for the off-normal measurements. In both cases, the first monochromator crystal was miscut to enhance incident beam collimation. The reflectivity curve of the sample crystal and the Co  $K_\alpha$  fluorescence signal from the surface were simultaneously recorded with a photodiode detector and an energy-dispersive solid-state detector, respectively.

The polarization-dependent SEXAFS measurements were performed with a double-crystal Ge(111) monochromator. The x-rays were incident on the surface at an angle of about 8°, with the electric vector polarized in the surface in-plane direction for the in-plane measurement, and in the surface normal direction for the out-of-plane measurements. EXAFS data were collected in fluorescence mode using a solid-state detector on the Co  $K_\alpha$  fluorescence emission. Data for the reference compound of powdered sphaerocobaltite  $\text{CoCO}_3$ , which has identical bonding structures and crystallographic symmetry as calcite, were acquired in transmission mode with a photodiode detector. For both XSW and SEXAFS measurements, the monochromator was detuned to about 75% of its peak intensity, and its output was monitored with an ion chamber.

## III. RESULTS

### A. XSW results

The Bragg-reflection XSW technique<sup>19</sup> is a high-resolution structural probe effective for locating the site of a

surface impurity relative to a bulk crystal lattice.<sup>17</sup> A combination of three XSW measurements made using mutually noncollinear diffraction vectors can give the unambiguous three-dimensional position of the impurity atom.<sup>18</sup> XSW has been used to determine impurity ion surface structures on the calcite surface in a number of previous studies.<sup>12–14,20</sup>

For the Bragg case of the dynamical x-ray diffraction,<sup>21</sup> the standing wave field generated inside the crystal<sup>22</sup> extends to above the crystal surface.<sup>17</sup> This XSW field has a period equal to the lattice spacing  $d_H$  of the diffraction planes  $H = hki$ . The position of the XSW antinodes relative to the diffraction planes, or phase  $\nu$ , may be varied by changing the x-ray incident angle  $\theta$  through the Darwin curve of a Bragg reflection. The characteristic modulation of the fluorescence yield from a given atomic species as a function of  $\theta$  is specific for the atomic position relative to the bulk diffraction planes, and for its distribution about this position. This normalized fluorescence yield function is

$$Y(\theta) = 1 + R(\theta) + 2\sqrt{R(\theta)}f_H \cos[\nu(\theta) - 2\pi P_H]. \quad (1)$$

In this equation, the reflectivity  $R(\theta)$  and the XSW phase  $\nu(\theta)$  are derived from the dynamical diffraction theory. The coherent fraction  $f_H$  and the coherent position  $P_H$  for the  $H$  diffraction planes of the substrate crystal lattice represent, respectively, the amplitude and phase of the  $H$  Fourier component of the spatial distribution of the atomic species. As fitting parameters in Eq. (1),  $P_H$  gives the  $\Delta d_H/d_H$  position, and  $f_H$  gives the static and dynamic spread of the atomic distribution. They are obtained from a best  $\chi^2$  fit of Eq. (1) to the background-subtracted XSW data.

The XSW experimental results for  $\text{Co}^{2+}$  incorporation at the calcite (10 $\bar{1}$ 4) surface are shown in Fig. 1, which displays the experimental reflectivity  $R(\theta)$  and normalized Co  $K_\alpha$  fluorescence yields  $Y(\theta)$  for the (10 $\bar{1}$ 4), (01 $\bar{1}$ 8), and (2 $\bar{2}$ 04) measurements. The solid-line curves are the best fits of Eq. (1) to these data. The coherent fractions and coherent positions extracted from these fits are listed in the figure and in Table I. The total surface coverage of Co of this particular sample is  $0.05 \pm 0.02$  monolayer (ML); it was determined by comparing the off-Bragg Co  $K_\alpha$  fluorescence intensity with that of Ga  $K_\alpha$  from a Ga-implanted Si-substrate standard. This Co coverage value is within the typical range of coverages for Co-on- $\text{CaCO}_3$  samples prepared with the same method.

### B. SEXAFS results

The theory and technique of polarization-dependent SEXAFS are reviewed in Ref. 23. We are concerned here with only the first-shell bonding information of the coherently incorporated surface  $\text{Co}^{2+}$  and its nearest-neighbor O atoms of the surrounding  $\text{CO}_3^{2-}$  groups. For a single shell, the absorption function  $\chi(k)$  can be written as

$$\chi(k) = N|f(k)|\sin[2kR + \phi(k)]\exp(-2k^2\sigma^2). \quad (2)$$

The functions  $f(k)$  and  $\phi(k)$  are the first-shell components of the amplitude and phase of  $\chi(k)$ , respectively. The parameters  $N$ ,  $R$ , and  $\sigma$  are the first-shell coordination number, radial distance, and EXAFS Debye-Waller factor, respectively.

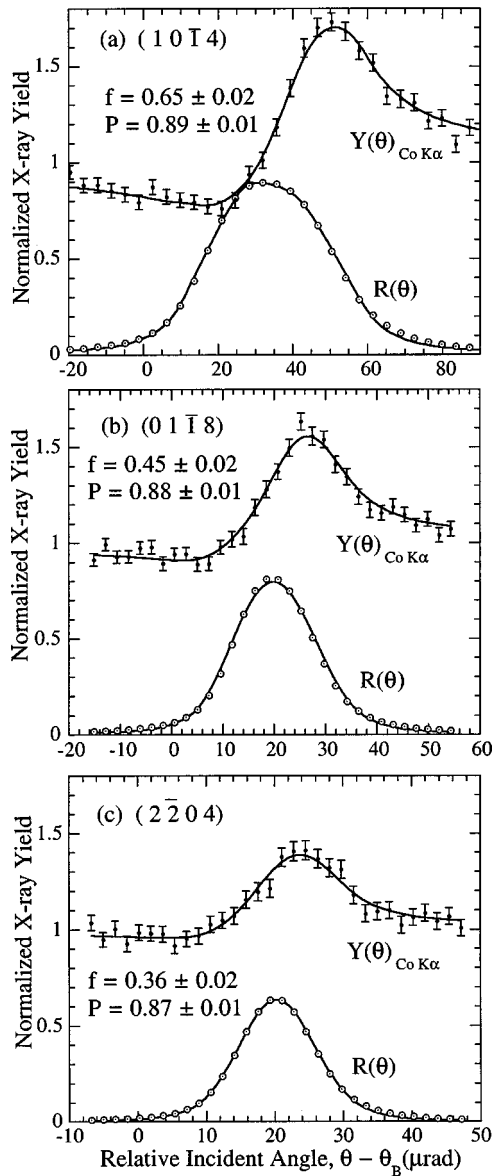


FIG. 1. XSW triangulation results. Experimental data (dots) and theoretical fits (solid-line curves) of the normalized x-ray reflectivity  $R$  and  $\text{Co } K_{\alpha}$  fluorescence yield  $Y$  for (a) the  $(10\bar{1}4)$ , (b) the  $(01\bar{1}8)$ , and (c) the  $(2\bar{2}04)$  Bragg reflections of calcite.

The background-subtracted,  $k^2$ -weighted EXAFS data from the in-plane and the normal polarization measurements of the sample surface, and that of the powdered  $\text{CoCO}_3$  reference compound, are shown as open circles in Fig. 2. Data were analyzed using the MACXAFS software<sup>24</sup> according to

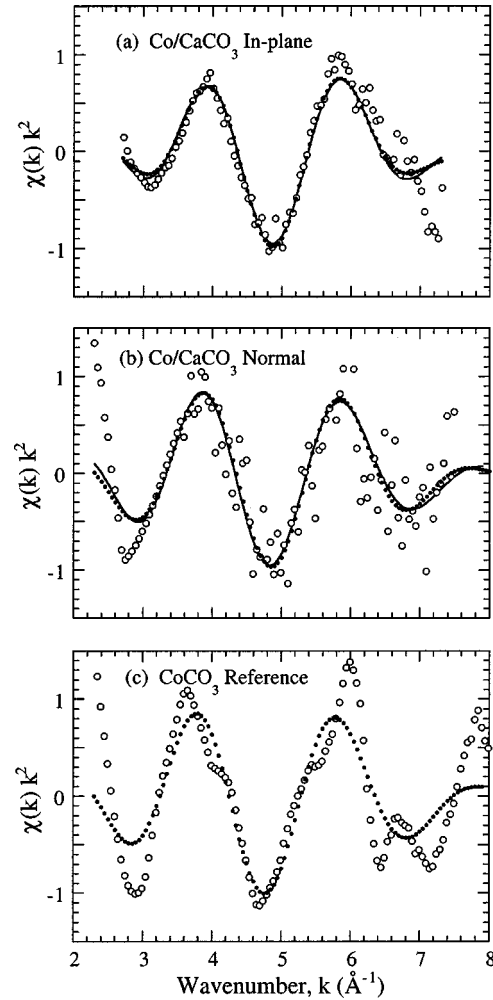


FIG. 2. Polarization-dependent SEXAFS results for Co incorporated at the calcite  $(10\bar{1}4)$  surface. Raw data after background subtraction (open circles), the  $\text{Co-O}$  first-shell component (dotted lines), and the best fit to the first-shell component (solid lines), shown in  $\chi(k)k^2$  as a function of  $k$ , for (a) the in-plane, (b) the out-of-plane polarization measurements, and (c) the  $\text{CoCO}_3$  standard compound.

standard procedures.<sup>25</sup> For the in-plane polarization data, the  $\chi(k)k^2$  data were Fourier transformed into  $R$  space over the range  $2.70 \leq k \leq 7.30 \text{ \AA}^{-1}$ , with modified Hanning windows of width  $0.40 \text{ \AA}^{-1}$ . The first-shell component of the Fourier-transformed data was filtered in the range  $0.58 \leq R \leq 2.55 \text{ \AA}$  with windows of  $0.30 \text{ \AA}$ . For the out-of-plane polarization data, the  $\chi(k)k^2$  data were forward transformed over the range  $2.30 \leq k \leq 7.90 \text{ \AA}^{-1}$  with windows of  $0.70 \text{ \AA}^{-1}$ . The

TABLE I. XSW coherent fractions and positions for Co incorporated at the calcite surface, and the Co positions derived from the coherent positions and according to the structural model.

| $H$            | $d_H (\text{\AA})$ | $f_H$           | XSW measured    |                    | Model              |              |
|----------------|--------------------|-----------------|-----------------|--------------------|--------------------|--------------|
|                |                    |                 | $P_H$           | $h_H (\text{\AA})$ | $h_H (\text{\AA})$ | $(\pm 0.04)$ |
| $(10\bar{1}4)$ | 3.04               | $0.65 \pm 0.02$ | $0.89 \pm 0.01$ | $2.70 \pm 0.03$    |                    |              |
| $(01\bar{1}8)$ | 1.91               | $0.45 \pm 0.02$ | $0.88 \pm 0.02$ | $1.68 \pm 0.04$    | 1.69               | 1.62         |
| $(2\bar{2}04)$ | 1.93               | $0.36 \pm 0.02$ | $0.87 \pm 0.02$ | $1.67 \pm 0.04$    | 1.72               | 1.54         |

TABLE II. Best-fit values for the Co-O first-shell EXAFS parameters for the in-plane and normal Co-on-CaCO<sub>3</sub> measurements.

|          | $N$           | $R$ (Å)         | $\Delta\sigma^2$ (Å <sup>2</sup> ) | $\Delta E$ (eV) |
|----------|---------------|-----------------|------------------------------------|-----------------|
| In-plane | $4.0 \pm 0.7$ | $2.11 \pm 0.02$ | $0.003 \pm 0.003$                  | -3.5            |
| Normal   | $1.9 \pm 0.4$ | $2.10 \pm 0.02$ | $0.001 \pm 0.002$                  | -1.7            |

first-shell component was filtered in the range  $0.67 \leq R \leq 2.43$  Å with windows of 0.24 Å. Corresponding processing was done with identical window parameters for the reference CoCO<sub>3</sub> data. The filtered first-shell components from the total data are shown as dotted lines in Fig. 2. The first-shell fits were made with respect to that of the CoCO<sub>3</sub> standard data. The best fits for the two polarizations are shown as solid lines in Fig. 2.

The best-fit parameters are obtained by minimizing the normalized  $\chi^2$  value, defined as the difference in phase and amplitude of the filtered first-shell data and fit. The fitting parameters allowed to vary while determining the best fit were  $R$ ,  $N$ ,  $\Delta\sigma^2$  (the difference in  $\sigma^2$  between the sample and the standard), and the energy shift variable  $\Delta E$ . The best-fit values for these parameters are listed in Table II. The uncertainties in  $R$  and  $\Delta\sigma^2$  were each obtained by doubling the  $\chi^2$  value while allowing other parameters to vary. The uncertainty in  $N$  was estimated to be  $1/6N$  ( $N=6$  for octahedral coordination); this estimate gives larger, more realistic values than residue doubling. The  $N$  and their uncertainty values listed in Table II have been polarization normalized to account for a maximum allowed in-plane Co-O coordination number of 4, and normal coordination number of 2.

#### IV. DISCUSSION

##### A. XSW: Co lattice sites

The calcite (10 $\bar{1}$ 4) surface has been shown by a number of recent atomic force microscopy studies to be highly ordered in aqueous environment<sup>26,27</sup> and in vacuo;<sup>28</sup> the in-plane surface unit cell has essentially the bulk calcite symmetry and cell parameter values. Under certain aqueous conditions, limited vertical relaxations of Ca<sup>2+</sup> and CO<sub>3</sub><sup>2-</sup> ions at the calcite-water interface were both predicted<sup>29</sup> and observed,<sup>30</sup> but without reconstruction or disordering. The Ca<sup>2+</sup> ion is octahedrally coordinated to O atoms of six adjacent CO<sub>3</sub><sup>2-</sup> groups, four of which are in the (10 $\bar{1}$ 4) plane.

From the XSW-measured coherent positions, the projected height  $h_H$  of the mean Co<sup>2+</sup> position relative to the  $H$  diffraction planes in the plane normal direction can be calculated with the equation

$$h_H = P_H \times d_H. \quad (3)$$

Accordingly, the projected heights of Co<sup>2+</sup> in the [10 $\bar{1}$ 4], [01 $\bar{1}$ 8], and [2 $\bar{2}$ 04] directions are  $h_{10\bar{1}4} = 2.70 \pm 0.03$  Å,  $h_{01\bar{1}8} = 1.68 \pm 0.04$  Å, and  $h_{2\bar{2}04} = 1.67 \pm 0.04$  Å. To locate the lattice sites of Co<sup>2+</sup>, we compare these  $h_H$  values with the corresponding  $h_H$  values for the ideal Ca<sup>2+</sup>, which are zero Å for all three  $H$ . This indicates that the Co<sup>2+</sup> ion is displaced from the ideal Ca<sup>2+</sup> site, or relaxed. The magnitude of this displacement, however, is small in comparison to

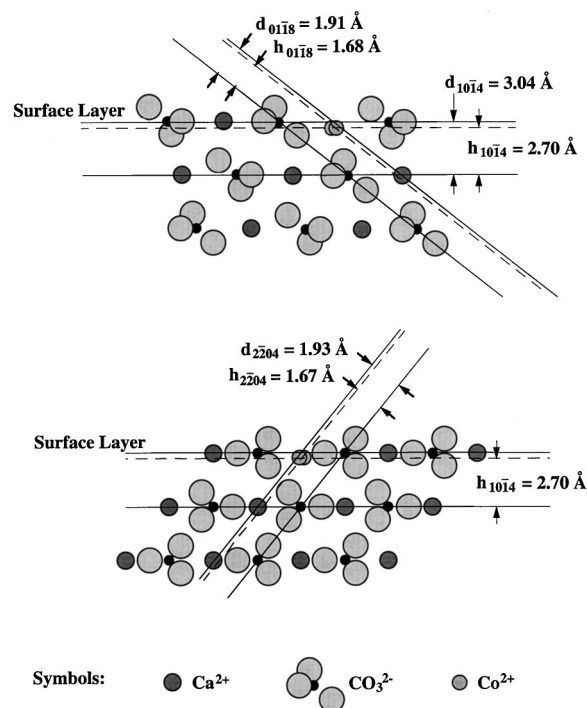


FIG. 3. Side views of the calcite (10 $\bar{1}$ 4) surface showing the averaged height  $h_H$  of Co<sup>2+</sup> with respect to the three lattice planes according to XSW measurements, and the positions of the two crystallographically nonequivalent Co<sup>2+</sup> ions according to the structural model.

the Ca-O nearest-neighbor bond distance of 2.35 Å, such that the Co<sup>2+</sup> ion is still located within the volume of the ideal CaO<sub>6</sub> octahedron. A model showing the substitutional Co<sup>2+</sup> structure according to the XSW data is shown in Fig. 3. This structure is in agreement with the substitutional structures of Pb<sup>2+</sup> and Zn<sup>2+</sup> at the calcite (10 $\bar{1}$ 4) surface.<sup>13,14</sup>

##### B. SEXAFS: Co bonding structure

The measured in-plane coordination number  $N=4.0 \pm 0.7$  and out-of-plane coordination number  $N=1.9 \pm 0.4$  indicate that the Co<sup>2+</sup> ion is bonded in a fully occupied CoO<sub>6</sub> octahedron, which, according to XSW results, is located at the surface CaO<sub>6</sub> octahedral site. The size of the surface CoO<sub>6</sub> octahedron, with  $R_{\text{Co-O}} = 2.10$  or 2.11 Å, is the same as that of CoO<sub>6</sub> in sphaerocobaltite CoCO<sub>3</sub>, where the first-neighbor Co-O distance is 2.10 Å,<sup>31</sup> but substantially smaller than that of CaO<sub>6</sub>, where the Ca-O distance is 2.36 Å.

A Co<sup>2+</sup> ion located in the top monolayer of an ideally truncated calcite (10 $\bar{1}$ 4) surface would be bonded vertically only with an O atom in the second layer, i.e.,  $N \sim 1$ . The most plausible interpretation for the observed out-of-plane coordination number of  $N=1.9 \pm 0.4$  is that the Co<sup>2+</sup> ion is in addition bonded to an O-bearing coadsorbate above itself. This explains how the Co<sup>2+</sup> ion maintains its preferred octahedral coordination at a surface site. A likely candidate for this coadsorbate species is the hydroxyl group that has remained bonded to the surface Co<sup>2+</sup> ion after removal of the adsorption solution. The hypothesis of a hydroxyl coadsorbate is based on the observation that water molecules are

attached to the surface cation while the calcite surface is in an aqueous environment,<sup>30</sup> and is consistent with bond length considerations, since the vertical distance  $R_{\text{Co-O}} = 2.10 \pm 0.02 \text{ \AA}$  is that of the first-neighbor Co-O distance in the hydrated  $\text{Co}(\text{OH})_6^-$  complex, or  $2.09 \text{ \AA}$ .<sup>33</sup>

It should also be noted that there is a consistent Co-O distance, of  $2.09\text{--}2.11 \text{ \AA}$ , for the preferred octahedral coordination of  $\text{Co}^{2+}$  with inorganic oxyanions; this is observed in the crystalline  $\text{CoCO}_3$ ,<sup>31</sup> the  $\text{Co}(\text{OH})_6^-$  hydration sphere,<sup>33</sup> Co surface phases,<sup>32</sup> and Co as a bulk impurity in calcite.<sup>1</sup> This fact is useful in interpreting the present SEXAFS data; for a typical Co-on- $\text{CaCO}_3$  sample surface contains both coherent (substitutional  $\text{Co}^{2+}$ ) and incoherent (randomly adsorbed Co) phases, and often the incoherent phase cannot be considered negligible in coverage. A quantitative measure of the coverage ratio of the coherent to the incoherent phases can be obtained from the XSW coherent fraction. The Co surface samples used in these SEXAFS measurements had normal XSW coherent fraction of  $f_{10\bar{1}4} = 0.40\text{--}0.65$ . The unavoidable inclusion of the random phase in the total SEXAFS data, however, does not cause practical difficulties in analyzing and interpreting the coherent portion of the data, since the random phase, according to the foregoing discussion, is expected to have the same  $R_{\text{Co-O}}$  and  $N$  values as the coherent phase (although this is not necessarily true for  $\sigma^2$ ).

### C. Structural model

To first approximation, we attribute the structural deviation of the surface  $\text{Co}^{2+}$  from the ideal  $\text{Ca}^{2+}$  to two dominant forces. The first is the radial-directional Coulomb force between  $\text{Co}^{2+}$  and its negatively charged first-neighbor O atoms of the  $\text{CO}_3^{2-}$  anions, due to the smaller size of the  $\text{Co}^{2+}$  ion. The second is the normal-direction relaxation (or expansion) of the surface, due to lattice asymmetry. We further divide the vertical relaxation of the surface  $\text{Co}^{2+}$  into two components: that in the top lattice layer and that in all sublayers. We may represent the former by a reduction in the vertical Ca-O bond length, and the latter by a vertical displacement of the second-layer O atoms on which the vertical Co-O bonds are anchored.

A structural model for the surface  $\text{Co}^{2+}$  impurity ion can be constructed according to these assumptions, and quantified using structural parameters from the experiments. In particular, the XSW and SEXAFS data include independent measurements of four vertical-position-sensitive parameters of the surface  $\text{Co}^{2+}$  ion; they are  $h_{10\bar{1}4}$ ,  $h_{01\bar{1}8}$ ,  $h_{22\bar{0}4}$ , and the vertical  $R_{\text{Co-O}}$ . We may quantify the model using  $h_{10\bar{1}4}$  and  $R_{\text{Co-O}}$ , and test the model by using it to calculate  $h_{01\bar{1}8}$  and  $h_{22\bar{0}4}$ , and compare the calculated and the experimental values.

Referring to Fig. 4, when  $\text{Ca}^{2+}$  is substituted with  $\text{Co}^{2+}$  at the surface cation site, the vertical cation-to-oxygen distance is reduced from  $R_{\text{Ca-O}}$  ( $2.35 \text{ \AA}$ ) to  $R_{\text{Co-O}}$  ( $2.10 \text{ \AA}$ ). The vertical displacement of the second-layer O atoms of the Co-O bonds was not experimentally determined, but it can be solved using experimentally determined quantities and the calcite structure parameters. If we represent the vertical displacement of the O atoms from their bulk-symmetry posi-

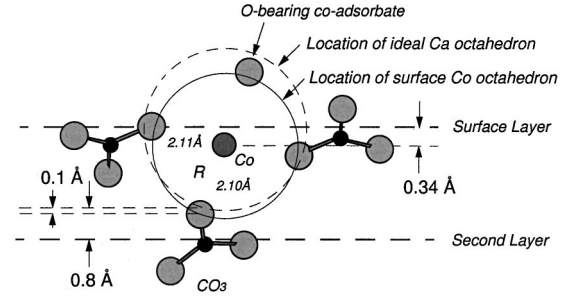


FIG. 4. Side view of a model describing the local structure of the  $\text{Co}^{2+}$  ion incorporated at the calcite ( $10\bar{1}4$ ) surface.

tions as  $\Delta O$ , the following relation (in  $\text{\AA}$  units) describes the vertical lattice position of the  $\text{Co}^{2+}$  ion:

$$h_{10\bar{1}4} = (R_{\text{Co-O}} \hat{R} \cdot \hat{n}_{10\bar{1}4}) - \Delta O + 0.8, \quad (4)$$

where  $\hat{R}$  represents the unit vector of the vertical cation-to-oxygen bond,  $\hat{n}_{10\bar{1}4}$  the unit vector of the ( $10\bar{1}4$ ) surface normal, and the value 0.8 is the projected height of the bulk-symmetry O atoms above the ( $10\bar{1}4$ ) plane in  $\text{\AA}$  units. (Since the two nonequivalent vertical Ca-O bonds have identical projection in the surface normal direction, we will not distinguish them in this discussion.) With  $h_{10\bar{1}4} = 2.70 \text{ \AA}$  and  $R_{\text{Co-O}} = 2.10 \text{ \AA}$ , Eq. (4) gives  $\Delta O = -0.1 \text{ \AA}$ , or the second-layer O atom is relaxed toward the bulk by a distance of  $0.1 \text{ \AA}$ .

To test this structural model, we used it to find the values of  $h_{01\bar{1}8}$  and  $h_{22\bar{0}4}$  for  $\text{Co}^{2+}$  and compare them to the experimental values. Note that an equal amount of relaxation in the two nonequivalent vertical cation-to-oxygen bonds does not project an equal distance along an arbitrary lattice plane axis (see Fig. 3). Therefore, the relaxed  $\text{Co}^{2+}$  ions have two different  $h_H$  values for an off-normal  $H$ , and the XSW-measured  $h_H$  value in such a case is the average of the two (given that the difference in the two  $h_H$  values is small). The averages of the model-determined  $h_{01\bar{1}8}$  and  $h_{22\bar{0}4}$  values are compared with the respective experimental values in Table I; they show good agreement.

### D. The role of the carbonate molecule in cation incorporation on calcite

The  $\text{Co}^{2+}$ -incorporated calcite ( $10\bar{1}4$ ) surface lattice observed here can be viewed as a dilute two-dimensional solid solution with mixing ratio 0.05, or  $\text{Co}_{0.05}\text{Ca}_{0.95}\text{CO}_3$ . Using the analogy of bulk solid-solution analysis,<sup>8</sup> the near-neighbor structure for an impurity  $M$  in the calcite ( $10\bar{1}4$ ) lattice can be characterized by a dimensionless relaxation parameter

$$\epsilon = (R_{M-O} - R_{\text{Ca-O}}^0) / (R_{M-O}^0 - R_{\text{Ca-O}}^0), \quad (5)$$

where the superscript zero denotes the near-neighbor distances in pure crystals. For the  $\text{Co}_{0.05}\text{Ca}_{0.95}\text{CO}_3$  surface,  $\epsilon = 1$  (the Pauling limit) in the first neighbor according to our experimental results. For the in-plane first-neighbor structure of the  $\text{Zn}_{0.09}\text{Ca}_{0.91}\text{CO}_3$  and the  $\text{Pb}_{0.05}\text{Ca}_{0.95}\text{CO}_3$  surfaces,<sup>14,2</sup> we also obtain  $\epsilon = 1$  (the out-of-plane measurements on these surfaces were not made). Since a relaxation parameter  $\epsilon \approx 1$

describes impurities in the calcite bulk,<sup>1-3</sup> it indicates that the origin of this relaxation is mainly not a surface effect, but some strain relaxation mechanism intrinsic to the calcite structure.

In investigation of the bulk  $\text{Co}^{2+}$  impurities, it was revealed that the radial distances for the C atom and for the second-shell O atom in the  $\text{CO}_3^{2-}$  molecule adjacent to the impurity cation do not show substantial relaxations.<sup>1</sup> Using these outer-shell distance data, we obtain for the C atom a corresponding  $\epsilon=0.38$ ; and for the second-shell O atom,  $\epsilon=0.05$ , a value approaching the VCA limit. These calculations indicate that the  $\text{CO}_3^{2-}$  molecules more or less remain at their pure calcite lattice sites, but are effectively "stretched" in the radial direction of the impurity. In other words, the  $\epsilon=1$  relaxation of the first-neighbor O atom is apparently achieved by an internal reformation of the  $\text{CO}_3^{2-}$  molecule, through such mechanisms as molecular rotation and covalent bond bending, for example. This repertoire of intramolecular potentials may be selectively raised so that the total energy of the impurity site is minimized. The dominant component of the calcite lattice energy is the interatomic Madelung energy,<sup>34</sup> of which the Coulomb interactions among first neighbors account for a significant fraction; the reaching of the Pauling limit of the first-neighbor distance is an indication that an optimized structure for minimizing this fraction of the lattice energy is achieved.

Structural relaxation executed by intramolecular potentials is a unique property of molecular ionic crystals. In monatomic crystals, in contrast, relaxation at impurity sites is limited. For example, in alkali halide-type binary ionic solid solutions, relaxation resorts to local buckling of the crystal lattice,<sup>35</sup> and the first-neighbor relaxation achieved is  $\epsilon \approx 0.5$  at the impurity limit.<sup>4,5</sup> Similarly, for binary covalent alloys,  $\epsilon=0.6-0.8$  is observed or predicted at the impurity limit for a variety of crystals.<sup>7-9</sup>

The simultaneous fulfillment of both the local chemical bonding for the impurity ion (i.e.,  $\epsilon=1$  in the first-neighbor and octahedral coordination) and the long-range order for the host lattice (i.e., the first-neighbor  $\text{CO}_3^{2-}$  molecules remain at pure-lattice sites) is the structural basis of isomorphic cation incorporation at the calcite surface. Note that such incorporation has been observed for ions whose  $M$ -O distances in their respective pure carbonates are substantially different from  $R_{\text{Ca-O}}^0$  (for  $\text{Co}^{2+}$ , the ratio of  $M$ -O distances in pure crystals is  $R_{\text{Co-O}}^0/R_{\text{Ca-O}}^0=0.89$ ; for  $\text{Pb}^{2+}$ ,  $R_{\text{Pb-O}}^0/R_{\text{Ca-O}}^0=1.14$ ). This extraordinary structural property of the calcite surface is either enabled or greatly enhanced by the capability of internal morphological reformation of the  $\text{CO}_3^{2-}$  molecule, which helps both accommodate the impurity ion and absorb the lattice strain it induces.

In summary, we have combined XSW triangulation and polarization-dependent SEXAFS to determine the lattice sites and local bonding structures of an impurity  $\text{Co}^{2+}$  ion incorporated at the calcite (10 $\bar{1}$ 4) surface lattice. From this and other related calcite surface impurity structures, we attribute isomorphic cation incorporation by the calcite surface to a large extent to the capacity for intramolecular reformation of the carbonate molecules in the lattice.

#### ACKNOWLEDGMENTS

This work was supported by the U.S. Department of Energy, Office of Basic Energy Sciences, under Contract No. W-31-109-Eng-38 to Argonne National Laboratory, and was conducted at the National Synchrotron Light Source. We thank Paul Fenter and Kenneth Kemner for helpful discussions.

<sup>1</sup>R. J. Reeder, G. M. Lamble, and P. A. Northrup, *Am. Mineral.* **84**, 1049 (1999).

<sup>2</sup>L. Cheng, Ph.D. thesis, Northwestern University, 1998.

<sup>3</sup>N. E. Pingitore, F. W. Lytle, B. M. Davies, M. P. Eastman, P. G. Eller, and E. M. Larson, *Geochim. Cosmochim. Acta* **56**, 1531 (1992).

<sup>4</sup>J. B. Boyce and J. C. Mikkelsen, *Phys. Rev. B* **31**, 6903 (1995).

<sup>5</sup>H. Sato, T. Yokoyama, I. Ono, K. Kaneyuki, and T. Ohta, *Jpn. J. Appl. Phys., Part 1* **31**, 1118 (1992).

<sup>6</sup>A. Frenkel, E. A. Stern, A. Voronel, M. Qian, and M. Newville, *Phys. Rev. B* **49**, 11 662 (1994).

<sup>7</sup>J. C. Mikkelsen and J. B. Boyce, *Phys. Rev. B* **28**, 7130 (1983).

<sup>8</sup>J. L. Martins and A. Zunger, *Phys. Rev. B* **30**, 6217 (1984).

<sup>9</sup>J. C. Woicik, K. E. Miyano, C. A. King, R. W. Johnson, J. G. Pellegrino, T.-L. Lee, and Z. H. Lu, *Phys. Rev. B* **57**, 14 592 (1998).

<sup>10</sup>M. Exner, H. Donnerberg, C. R. A. Catlow, and O. F. Schirmer, *Phys. Rev. B* **52**, 3930 (1995).

<sup>11</sup>W. Stumm, *Chemistry of the Solid-Water Interface* (Wiley, New York, 1992).

<sup>12</sup>Y. Qian, N. C. Sturchio, R. P. Chiarello, P. F. Lyman, T.-L. Lee, and M. J. Bedzyk, *Science* **265**, 1555 (1994).

<sup>13</sup>N. C. Sturchio, R. P. Chiarello, L. Cheng, P. F. Lyman, M. J.

Bedzyk, Y. Qian, H. You, D. Yee, P. Geissbuhler, L. Sorensen, Y. Liang, and D. Baer, *Geochim. Cosmochim. Acta* **61**, 251 (1997).

<sup>14</sup>L. Cheng, N. C. Sturchio, J. C. Woicik, K. M. Kemner, P. F. Lyman, and M. J. Bedzyk, *Surf. Sci.* **415**, L976 (1998).

<sup>15</sup>R. J. Reeder, *Geochim. Cosmochim. Acta* **60**, 1543 (1996).

<sup>16</sup>R. C. Chiarello, N. C. Sturchio, J. Grace, P. Geissbuhler, L. Sorensen, L. Cheng, and S. Xu, *Geochim. Cosmochim. Acta* **61**, 1467 (1997).

<sup>17</sup>P. L. Cowan, J. A. Golovchenko, and M. F. Robbins, *Phys. Rev. Lett.* **44**, 1680 (1980).

<sup>18</sup>J. A. Golovchenko, J. R. Patel, D. R. Kaplan, P. L. Cowan, and M. J. Bedzyk, *Phys. Rev. Lett.* **49**, 560 (1982).

<sup>19</sup>J. Zegenhagen, *Surf. Sci. Rep.* **18**, 199 (1993).

<sup>20</sup>L. Cheng, P. F. Lyman, N. C. Sturchio, and M. J. Bedzyk, *Surf. Sci.* **382**, L690 (1997).

<sup>21</sup>B. W. Batterman and H. Cole, *Rev. Mod. Phys.* **36**, 681 (1964).

<sup>22</sup>B. W. Batterman, *Phys. Rev. Lett.* **22**, 703 (1969).

<sup>23</sup>J. Stöhr, in *X-Ray Absorption*, edited by D. C. Koningsberger and R. Prins (Wiley, New York, 1988).

<sup>24</sup>C. Bouldin, L. Furenlid, and T. Elam, *Physica B* **208-209**, 190 (1995).

<sup>25</sup>D. E. Sayers and B. A. Bunker, in *X-Ray Absorption* (Ref. 23).

- <sup>26</sup>F. Ohnesorge and G. Binnig, *Science* **260**, 1451 (1993).
- <sup>27</sup>Y. Liang, A. S. Lea, D. R. Baer, and M. H. Engelhard, *Surf. Sci.* **351**, 172 (1996).
- <sup>28</sup>S. L. S. Stipp and M. F. Hochella, Jr., *Geochim. Cosmochim. Acta* **55**, 1723 (1991).
- <sup>29</sup>N. H. De Leeuw and S. C. Parker, *J. Chem. Soc., Faraday Trans.* **93**, 467 (1997).
- <sup>30</sup>P. Fenter, P. Geissbuhler, E. DiMasi, G. Srajer, L. Sorensen, and N. C. Sturchio, *Miner. Mag.* **62A**, 1471 (1998).
- <sup>31</sup>F. Pertlik, *Acta Crystallogr., Sect. C: Cryst. Struct. Commun.* **42**, 4 (1986).
- <sup>32</sup>S. N. Towle, J. Bargar, G. E. Brown, and G. A. Parks, *Physica B* **208-209**, 439 (1995).
- <sup>33</sup>M. Magini, *X-Ray Diffraction of Ions in Aqueous Solution* (CRD Press, Boca Raton, FL, 1988).
- <sup>34</sup>R. K. Singh and N. K. Gaur, *Phys. Rev. B* **35**, 4462 (1987).
- <sup>35</sup>A. Frenkel, E. A. Stern, A. Voronel, M. Qian, and M. Newville, *Phys. Rev. Lett.* **71**, 3485 (1993).